Heliyon 8 (2022) e12312

Contents lists available at ScienceDirect

Heliyon

journal homepage: www.cell.com/heliyon

Research article

Paeoniflorin alleviates inflammatory response in IBS-D mouse model via downregulation of the NLRP3 inflammasome pathway with involvement of miR-29a

Wei Ke [a,b,c,1], Yongfu Wang [d,1], Siyu Huang [a,b,e], Shan Liu [a,b,c], He Zhu [a,b], Xiangyu Xie [a,b,c], Huifei Yang [a,b,c], Qin Lu [a,b,c], Jianfeng Gan [a,b,c], Guodong He [a,b,c], Fei Che [a,f], Xin Wan [a,b,c], Hongmei Tang [b,*]

[a] The First Clinical Medical College of Guangzhou University of Chinese Medicine, Guangzhou 510405, China
[b] The First Affiliated Hospital of Guangzhou University of Chinese Medicine, Guangzhou 510405, China
[c] Lingnan Medical Research Center, Guangzhou University of Chinese Medicine, Guangzhou 510405, China
[d] Department of Traditional Chinese Medicine, The First Affiliated Hospital of Zhengzhou University, Zhengzhou, Henan 450052, China
[e] Guangdong Provincial Key Laboratory of Advanced Drug Delivery Systems and Guangdong Provincial Engineering Center of Topical Precise Drug Delivery System, Guangdong Pharmaceutical University, Guangzhou 510006, Guangdong, China
[f] Guangzhou Liwan District Hospital of Traditional Chinese Medicine, Guangzhou 510160, Guangdong, China

HIGHLIGHTS

- Paeoniflorin alleviated inflammatory response in IBS-D by downregulating miR-29a expression.
- Paeoniflorin inhibited the abnormal activation of the NLRP3 inflammasome pathway.
- After paeoniflorin treatment, damaged intestinal epithelial barrier was restored.

GRAPHICAL ABSTRACT

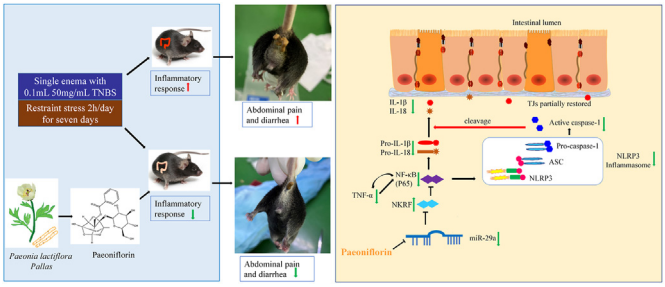

ARTICLE INFO

Keywords:
Paeoniflorin
irritable bowel syndrome
miR-29a
NLRP3 inflammasome

ABSTRACT

Paeoniflorin has been traditionally used to treat pain and immunologic derangement in China. However, its detailed mechanism remains to be illuminated. We investigated the mechanism by which paeoniflorin alleviates the inflammatory response in a mouse model of irritable bowel syndrome with predominant diarrhea (IBS-D). C57BL/6 wild type (WT) and miR-29a knockout (KO) mice were randomly divided into control, model, rifaximin, and paeoniflorin groups (n = 7). IBS-D model was induced by single intracolonic instillation of 0.1 mL trinitrobenzene-sulfonic acid (TNBS, 50 mg/mL) combined with restraint stress for seven consecutive days. The treatment groups received rifaximin (100 mg/kg) and paeoniflorin (50 mg/kg) via intragastric administration for seven days, respectively. The results showed that the fecal water content, fecal pellet output, visceral sensitivity, and histopathological score after paeoniflorin treatment were lower than those of the model group in both WT and miR-29a KO mice ($P < 0.05$). In both lineage mice, damage was observed in the colon tissues of model group, while paeoniflorin treatment partially ameliorated the tissue damage. Serum levels of DAO, DLA, IL-1β, IL-18,

* Corresponding author.
E-mail address: tanghongmei2000@163.com (H. Tang).
[1] The two authors contributed equally to this work and should be considered co-first authors.

https://doi.org/10.1016/j.heliyon.2022.e12312
Received 3 November 2022; Received in revised form 23 November 2022; Accepted 6 December 2022

TNF-α, and MPO were decreased after paeoniflorin treatment ($P < 0.05$), with miR-29a KO mice in a lower level compared with that of WT mice. RT-PCR showed that the relative expression of miR-29a, NF-κB (p65), NLRP3, ASC, caspase-1, IL-1β, and TNF-α was downregulated while NKRF was upregulated after paeoniflorin treatment ($P < 0.05$). Immunohistochemistry showed that intestinal epithelial protein levels of NLRP3, ASC, and caspase-1 decreased while those of Claudin-1 and ZO-1 increased in the paeoniflorin treatment group ($P < 0.05$). In general, compared with WT mice, NLRP3 inflammasome pathway targets was in much lower expression level than miR-29a KO mice. In conclusion, paeoniflorin could inhibit abnormal activation of the NLRP3 inflammasome pathway by inhibiting miR-29a in IBS-D, thereby relieving the inflammatory response of the intestinal mucosa and reconstructing the intestinal epithelial barrier.

1. Introduction

Irritable bowel syndrome (IBS) is a prevalent functional gastrointestinal disorder worldwide, characterized by recurrent abdominal pain associated with defecation or altered bowel habits [1]. As the most common subtype [2], IBS with predominant diarrhea (IBS-D) severely affects patients' quality of life and poses a heavy economic burden on patients and the healthcare system [3]. The etiopathogenesis of IBS-D is complex and may be associated with visceral hypersensitivity, immune dysregulation, intestinal barrier dysfunction, enteric dysbacteriosis, and psychological factors [4]. Unfortunately, few treatments have induced satisfactory therapeutic effects in patients with IBS-D [5]. Elucidating the molecular mechanism underlying IBS-D is needed to develop better treatment strategies.

Recent studies have demonstrated that low-grade intestinal inflammation with subsequent immune activation of the intestinal mucosa may be critical in the etiopathogenesis of IBS-D [6, 7, 8]. Indeed, immune activation is associated with the inflammatory response and visceral hypersensitivity in IBS [4, 9]. Inflammasomes play a key role in mucosal immunological regulation, among which the nucleotide oligomerization domain (NOD)-like receptor family pyrin domain-containing 3 (NLRP3) inflammasome has been thoroughly investigated [10]. Several studies have indicated that NLRP3 plays a critical role in intestinal innate immunity and gut homeostasis [10, 11]. NLRP3 inflammasomes can facilitate the maturation of pro-IL-1β and pro-IL-18 to form IL-1β and IL-18, respectively, when triggered by inflammatory stimuli, which subsequently leads to inflammatory reactivation [12, 13]. Abnormal inflammatory responses and immune activation can also lead to intestinal dysfunction and damage to the intestinal epithelial barrier, which is composed of multi-protein complexes consisting of the tight junction proteins claudin-1 and zonula occulens-1 (ZO-1). This eventually results in exposure to harmful antigens and microorganisms, which disrupts gut homeostasis [14, 15]. Rifaximin, a non-absorbable antibiotic, has proven to be effective against global symptoms and bloating in patients with IBS [16]. A previous study reported that rifaximin could alter the intestinal microbiota and prevent IBS-related symptoms [17]. Therefore, rifaximin was selected as the positive control in the current study.

MicroRNAs (miRNAs) regulate the expression of many genes participating in functional interaction pathways, through which they play important roles in pathophysiological functions [18]. The expression of miRNA-29a was reportedly increased in the colonic tissue of patients with IBS-D, and miRNA-29a was shown to target NF-κB-repressing factor (NKRF), thereby increasing intestinal permeability in patients with IBS [19, 20]. Moreover, NKRF is a key factor in priming the activation of NLRP3 inflammasomes, thus, precisely regulating NLRP3 expression [21]. Although the NLRP3 inflammasome pathway is reportedly involved in IBS-D [11], the role of miRNA-29a in intestinal immune homeostasis and intestinal epithelial barrier function in IBS-D is yet to be investigated.

Paeoniflorin is the main bioactive component in the root of *Paeonia lactiflora* Pall., which has long been used in traditional Chinese medicine formulations such as Tong Xie Yao Fang and Tong Xie Ning to treat symptoms of IBS such as abdominal pain and diarrhea [22, 23]. Previous studies have reported that paeoniflorin treatment ameliorated experimental colitis by regulating the gut microbiome [24, 25] and prevented intestinal barrier disruption by inhibiting the inflammatory response [26]. Paeoniflorin has also been shown to have an analgesic effect on visceral hyperalgesia in IBS-D model rats [27]. However, the molecular mechanism underlying the effectiveness of paeoniflorin against IBS-D remains unclear.

Therefore, the aim of this study was to investigate the therapeutic mechanism of paeoniflorin in mouse model of IBS-D induced by trinitrobenzene sulfonic acid (TNBS) enema combined with restraint stress, focusing on miR-29a and the NLRP3 inflammasome pathway.

2. Materials and methods

2.1. Reagents

Paeoniflorin (purity ≥98%) was purchased from Shanghai Macklin Biochemical Co., Ltd. (Shanghai, China; lot no. C12198153). Rifaximin was purchased from Alfasigma Pharmaceutical (Alanno, Italy; lot no. 22953). EVO M-MLV RT Premix and the SYBR® Green Premix Pro Taq HS qPCR kit for qPCR were obtained from Accurate Biotechnology Co., Ltd. (Changsha, China). The DL2000 Plus DNA Marker and DNA loading buffer were obtained from Vazyme Biotech Co. Ltd. (Nanjing, China). Primers for mmu-miR-29a-3p were synthesized by Accurate Biotechnology Co., Ltd. Primers for NLRP3, ASC, caspase-1, IL-1β, TNF-α, and β-actin were synthesized by Shanghai Generay Biotech Co. Ltd. (Shanghai, China).

2.2. Animals and genotype identification of miR-29a KO mice

This study was approved by the Animal Experimentation Ethics Committee of the International Institute for Translational Chinese Medicine, Guangzhou University of Chinese Medicine (certificate no. 2021W0039). Animal care and management protocols were carried out in accordance with the approved guidelines. The C57BL/6 wild-type (WT) mice were obtained from the Experimental Animal Center of Guangzhou University of Chinese Medicine (Guangzhou, China). The miR-29a$^{-/-}$ mice (miR-29a knockout [KO] mice) were generated and genotyped as previously described [28]. All mice were acclimated to the laboratory environment for one week prior to the experiments. The mice were maintained at 22 ± 1 °C and 50–70% humidity under a 12 h light-dark cycle with food and water provided ad libitum. Six-to-eight-week-old male mice weighing 20–25 g were selected for this study.

2.3. IBS-D mouse model and grouping

The IBS-D model was established in mice as previously reported, with certain adjustments [20, 29]. Briefly, mice were anesthetized with ether, their colons were instilled with 0.1 mL TNBS dissolved in 50% ethanol (50 mg/mL) 2 cm from the anus, and mice were held upside down for 30 s to prevent TNBS from leaking out. Subsequently, the upper forelimbs and thoracic trunks of the mice were wrapped with medical adhesive tape, which caused restraint stress but did not prevent bodily movement. The mice underwent restraint stress for 2 h per day for one week. Mice in the control group were instilled with 0.1 mL 50% ethanol without restraint stress. After confirmation of successful establishment of the IBS-D model, mice were allowed to recover for seven days before treatment.

C57BL/6 WT mice (n = 7) and miR-29a KO mice (n = 7) were randomly assigned to the control, IBS-D model, rifaximin, and paeoniflorin groups. Mice in the rifaximin and paeoniflorin groups received intragastric administration of rifaximin (100 mg/kg) and paeoniflorin (50 mg/kg), respectively, whereas mice in the control and IBS-D model groups received an equal volume of saline. The administration dosages of rifaximin and paeoniflorin were based on pre-experimental findings and previous studies [25, 30, 31]. After treatment, the diarrhea score, fecal water content, fecal pellet output, and visceral sensitivity were measured in each group. At the end of the study, the mice were anesthetized by isoflurane inhalation and their blood and colon tissue samples were collected for further use.

2.4. Diarrhea score and fecal water content

The diarrhea score was evaluated as previously described, with minor modifications [32]. Briefly, mice were placed in a metabolic cage for 1 h and fecal pellets were collected. Stool appearance was graded and scored by two blinded observers, as previously described [32]. The collected fecal pellets were weighed (wet weight) and dried at 60 °C for 24–48 h until they achieved constant weight (dry weight). The difference between the wet and dry weights was considered to be the fecal water content.

2.5. Fecal pellet output

After treatment, each mouse was placed in a restraint cage for 1 h at 25 ± 1 °C, which prevented free movement but did not restrict breathing. The fecal pellets excreted under 1 h restraint stress were collected and counted.

2.6. Visceral sensitivity

Visceral sensitivity was assessed as previously described [33]. Briefly, a 6F catheter was inserted into the mouse colon 2–3 cm from the anus to produce visceral pain via colorectal distension (CRD). Semi-quantitative abdominal withdrawal reflex (AWR) scores from 1 to 4 were used to evaluate the pain response when graded volumes (0.15, 0.30, 0.45, and 0.60 mL) of water were injected into the catheter [33]. Observers were blinded to the animal grouping and each mouse underwent CRD three times to calculate an average score and ensure accuracy.

2.7. Histological analysis

Mouse colon tissues were collected, fixed with 4% paraformaldehyde (Servicebio, Wuhan, China), and embedded in paraffin (Servicebio). A microtome (Leica, Wetzlar, Germany) was used to slice 5-μm sections. The sections were deparaffinized by soaking in xylene I for 20 min, xylene II for 20 min, absolute ethyl alcohol I for 5 min, absolute ethyl alcohol II for 5 min, 75 % ethyl alcohol for 5 min, and finally in distilled water for 5 min. The slices were stained with hematoxylin (Servicebio) for 3–5 min, rinsed with distilled water, decolorized in 1% hydrochloric ethanol solution, rinsed twice with distilled water, dehydrated with 85% ethyl alcohol for 5 min, dehydrated with 95% ethyl alcohol for 5 min, and then stained with eosin for 5 min. The dehydrated sections were rendered transparent by soaking in absolute ethyl alcohol I for 5 min, absolute ethyl alcohol II for 5 min, absolute ethyl alcohol III for 5 min, xylene I for 5 min, and xylene II for 5 min. The slices were sealed with neutral gum. The slices were viewed using a digital slide scanner (3DHISTECH, Budapest, Hungary) and scored by two observers blinded to the animal grouping, as previously described [34].

2.8. Ultrastructural observation by transmission electron microscopy (TEM)

TEM was conducted as previously reported [35]. Briefly, mouse colon tissues were fixed for 2–4 h in 2% glutaraldehyde at room temperature, followed by washing three times with 0.1 M phosphoric acid for 15 min each. The colon tissues were further fixed in 1% osmic acid and 0.1 M phosphate buffer (pH 7.4) at room temperature for 2 h, followed by washing three times with 0.1 M phosphoric acid for 15 min each. The tissues were dehydrated using an alcohol gradient. After embedding and polymerizing the tissues at 60 °C, the colon tissues were sectioned into 60–80 nm slices using an ultramicrotome (Leica). The slices were stained with uranyl acetate and lead citrate. Finally, the slices were examined using an HT7800/HT7700 TEM (Hitachi, Tokyo, Japan).

2.9. Enzyme-linked immunosorbent assay (ELISA)

Blood samples were collected and centrifuged at 1000 × *g* for 15 min at 4 °C to obtain the serum. Serum concentrations of diamine oxidase (DAO), D-lactate (D-LA), IL-1β, IL-18, TNF-α, and *myeloperoxidase* (MPO) were detected using individual ELISA kits following the manufacturer's instructions (Shanghai Jianglai Biotechnology Co., Ltd., Shanghai, China). Absorbance was measured at 450 nm using a microplate reader (Thermo Scientific, Multiskan GO, Waltham, MA, USA).

2.10. miRNA-29a target gene prediction and dual-luciferase assay

TargetScan (http://www.targetscan.org) and Mirbase (www.mirbase.org) were searched to predict the potential targets of miRNA-29a. For the dual-luciferase assay, NCM460 cells (obtained from Shanghai Yaji Biotechnology Co., LTD, Shanghai, China) were cultured in Dulbecco's Modified Eagle Medium (DMEM) in a 12-well plate with 1% penicillin (100 U/mL)/streptomycin (100 mg/mL) at 37 °C under a 5% CO_2 humidified atmosphere. The NCM460 cells were grown to 60% confluence before transfection. The NKRF 3′ UTR containing the miR-29a-3p binding site and its mutation fragment were inserted into the pmirGLO dual-luciferase miRNA target expression vector (Tsingke Biotechnology Co. Ltd., Beijing, China). The miR-29a-3p mimic or mimic control was co-transfected with the NKRF reporter construct (WT, mutant, or empty vector) into NCM460 cells. Luciferase activity was evaluated 24 h after transfection using the Dual-Glo Luciferase Assay System (Promega, Beijing, China) and normalized to that of Renilla luciferase activity.

2.11. RT-qPCR analysis of miRNA and mRNA

Total RNA from mouse colon tissue was extracted using TRIzol reagent (Invitrogen, Carlsbad, CA, USA). After extraction, RNA purity was determined via the ratio of absorbance at 260 nm (OD_{260}) and 280 nm (OD_{280}), using a NanoPhotometer-N50 microspectrophotometer (Implen, München, Germany). An OD_{260}/OD_{280} ratio in the range of 1.8–2.1 was considered to be acceptable. Reverse transcription of miR-29a was conducted using a first-strand synthesis kit (Takara Bio, Kusatsu, Japan) following the manufacturer's protocol. Amplification was performed using the SYBR® Green Premix Pro Taq HS qPCR kit (Accurate Biotechnology Co., Ltd.) and miR-29a expression was normalized to U6. cDNA was obtained by reverse transcription using EVO M-MLV RT Premix for qPCR (Accurate Biotechnology Co., Ltd.) for mRNA target analysis. RT-qPCR was performed on the Bio-Rad CFX96 Touch Real-Time PCR Detection System (Bio-Rad, Hercules, CA, USA) using the SYBR® Green Premix Pro Taq HS qPCR kit (Accurate Biotechnology Co., Ltd.). All reactions were performed in triplicate. mRNA expression was normalized to that of β-actin and calculated using the $2^{-\Delta\Delta Ct}$ method. The primers used for qRT-PCR are listed in Table 1.

2.12. Immunohistochemistry (IHC)

Immunohistochemical localization of NLRP3, ASC, caspase-1, claudin-1, and ZO-1 was performed as previously described [36]. Slices were incubated with the corresponding primary antibodies overnight at 4 °C: anti-NLRP3 (1:600; Servicebio; No. GB113000), anti-ASC (1:200; Cell

Table 1. Primer sequences for RT-qPCR.

Gene	Forward primer (5′ to 3′)	Reverse primer (3′ to 5′)
miR-29a-3p	TCGGTTAAGCACCATCTGAAA	AACGCTTCACGAATTTGCGT
NKRF	AGACCAGCCTGTAGCAACCAACAT	GCTTCTCGGCAACCAAGGACTCA
NFκB (p65)	AGGCTTCTGGGCCTTATGTG	TGCTTCTCTCGCCAGGAATAC
NLRP3	ATCAACAGGCGAGACCTCTG	GTCCTCCTGGCATACCATAGA
ASC	GACAGTGCAACTGCGAGAAG	CGACTCCAGATAGTAGCTGACAA
Caspase-1	CTTGGAGACATCCTGTCAGGG	AGTCACAAGACCAGGCATATTCT
IL-1β	GAAATGCCACCTTTTGACAGTG	TGGATGCTCTCATCAGGACAG
TNF-α	ACTCCAGGCGGTGCCTATGT	GTGAGGGTCTGGGCCATAGAA
U6	GGAACGATACAGAGAAGATTAGC	TGGAACGCTTCACGAATTTGCG
β-actin	GGGAAATCGTGCGTGAC	AGGCTGGAAAAGAGCCT

Signaling Technology, Boston, MA, USA; No. 66824), anti-caspase-1 (1:200; Proteintech, Chicago, IL, USA; No. 22915-1-AP), anti-claudin-1 (1:1000; Servicebio; GB112543), and anti-ZO-1 (1:500; Servicebio; No. GB111402). The IHC results were assessed based on densitometry using ImageJ software v1.8.0 (National Institutes of Health, Bethesda, MD, USA). Three or more images were captured for each slice to calculate the average densitometric value per mouse. The values for all mice in an experimental group were averaged as the group densitometry value.

2.13. Statistical analysis

The data were analyzed using IBM SPSS software v25.0 (IBM Corp., Armonk, NY, USA). Normal (Gaussian) distribution was determined for all datasets using the Shapiro–Wilk normality test. Datasets passing the normality test were expressed as the mean ± standard deviation (SD) and analyzed using one-way analysis of variance (ANOVA). The post hoc tests were performed using LSD-t when the variance is homogeneous or Dunnett's T3 when the variance is not homogeneous. Datasets where one (or more) group did not pass the normality test (assuming $\alpha = 0.05$) were analyzed using non-parametric tests (Kruskal-Wallis H test) followed by pairwise comparisons. Differences between WT and miR-29a KO groups were assessed using the unpaired t-test after the normality test. *P*-values <0.05 were considered to be statistically significant.

3. Results

3.1. Paeoniflorin treatment alleviates the main symptoms of IBS-D

To explore the therapeutic effect of paeoniflorin against IBS-D, macroscopic pathological indicators were measured in WT and miR-29a KO mice in each treatment group, including diarrhea score, fecal water content, fecal pellet output, and AWR under CRD. The diarrhea score was increased in the IBS-D model group compared to that in the control group ($P < 0.01$) and decreased in the rifaximin and paeoniflorin groups compared to that in the IBS-D model group ($P < 0.01$) (Figure 1a).

Compared to that in the control group, the fecal water content was higher in the IBS-D model group for both mouse lineages ($P_{all} < 0.01$) (Figure 1b) but lower in the rifaximin and paeoniflorin groups than in the IBS-D group for WT mice ($P_{rifaximin}<0.01$, $P_{paeoniflorin}<0.01$) and miR-29a KO mice ($P_{rifaximin}<0.05$, $P_{paeoniflorin}<0.05$) (Figure 1b). The diarrhea scores were consistent with the fecal water content values.

A previous study reported a clear correlation between colorectal hypersensitivity and fecal urgency among patients with diarrhea [37]. Therefore, intestinal sensitivity was assessed by fecal pellet output under restraint stress, as previously reported [38]. As demonstrated in Figure 1c, the stool frequency was increased in the IBS-D model group compared to that in the control group for both mouse lineages ($P_{all} < 0.01$) and decreased in the rifaximin and paeoniflorin groups compared to that in the IBS-D model group ($P_{all} < 0.01$) (Figure 1c).

AWR via CRD was employed to further measure intestinal sensitivity. As shown in Figure 1d, the IBS-D model group exhibited higher mean AWR scores than the control group for WT mice at all distention volumes ($P_{all} < 0.01$). Compared to the IBS-D model group, the rifaximin group exhibited lower mean AWR scores at distension volumes of 0.30 mL ($P < 0.01$) (Figure 1d); the paeoniflorin group exhibited lower mean AWR scores at distension volumes of 0.30 and 0.45 mL ($P_{all} < 0.05$) (Figure 1d). For miR-29a KO mice, the model group exhibited higher mean AWR scores than the control group at 0.15 and 0.30 mL distension volumes ($P < 0.05$) (Figure 1e). Compared to the IBS-D model group, the rifaximin group exhibited lower mean AWR scores at distension volume of 0.30 mL ($P < 0.05$) (Figure 1e); the paeoniflorin group exhibited lower mean AWR scores at distension volume of 0.15 and 0.45 mL ($P<0.05$) (Figure 1e). The AWR scores did not differ significantly in the rifaximin and paeoniflorin groups compared to those in the IBS-D model group at the distention volume of 0.60 mL (Figure 1e).

3.2. Paeoniflorin treatment remediates mouse colon tissue damage

The IBS-D model group exhibited obvious colon tissue damage compared to the control group for both WT and miR-29a KO mice (Figure 2a), which was characterized by loss of tissue structure, damage to mucosal glands, edema, and inflammatory cell infiltration. Tissue damage was significantly ameliorated in the rifaximin and paeoniflorin groups (Figure 2a). The histological scores were consistent with the microstructural observations for both mouse lineages (Figure 2b).

As shown in the TEM images (Figure 2c), the control group exhibited normal epithelial cells in the intestinal mucosa and strong, even staining of the junctional complexes for both WT and miR-29a KO mice. In addition, the microvilli in the control group were undamaged, neatly arranged, and clearly visible. In contrast, the epithelial cells were damaged and microvilli were sparsely arranged with uneven distribution and different lengths for both mouse lineages in the IBS-D group. Additionally, the junctional complexes were lightly and unevenly stained in the IBS-D group. However, microvilli and junctional complex integrity was restored to varying degrees in the rifaximin and paeoniflorin groups (Figure 2c).

3.3. Paeoniflorin treatment induces changes in DAO, D-LA, IL-1β, IL-18, TNF-α, and MPO serum levels

For WT mice, the IBS-D model group had higher serum DAO levels than the control group ($P < 0.01$), but the rifaximin and paeoniflorin groups had lower serum DAO levels than the IBS-D model group (both $P < 0.01$) (Figure 3a). For miR-29a KO mice, serum DAO levels did not differ among the groups ($P > 0.05$) (Figure 3a). Meanwhile, serum DAO levels were decreased in miR-29a KO mice compared to those in WT mice in the control and IBS-D model group ($P_{all} < 0.05$). Serum DAO levels did not differ between WT and miR-29a KO mice among the corresponding rifaximin, and paeoniflorin groups ($P > 0.05$) (Figure 3a).

For WT mice, serum D-LA levels were higher in the IBS-D model group than in the control group ($P < 0.01$) but were decreased in the rifaximin or paeoniflorin groups compared to those in the IBS-D group (both $P < 0.01$) (Figure 3b). Similarly, serum D-LA levels were higher in the IBS-D model group than in the control group for miR-29a KO mice ($P < 0.01$) but were decreased in the rifaximin and paeoniflorin groups compared to those in the IBS-D group (both $P < 0.01$) (Figure 3b). Additionally, WT mice in the IBS-D model and rifaximin groups had lower serum D-LA levels than those in the miR-29a KO mice among the corresponding groups ($P_{model}<0.05$ and $P_{rifaximin}<0.01$). Serum D-LA levels did not differ between WT and miR-29a KO mice in the control and paeoniflorin group ($P > 0.05$) (Figure 3b).

For both WT and miR-29a KO mice, serum IL-1β levels were higher in the IBS-D model group than in the control group ($P < 0.01$) (Figure 3c).

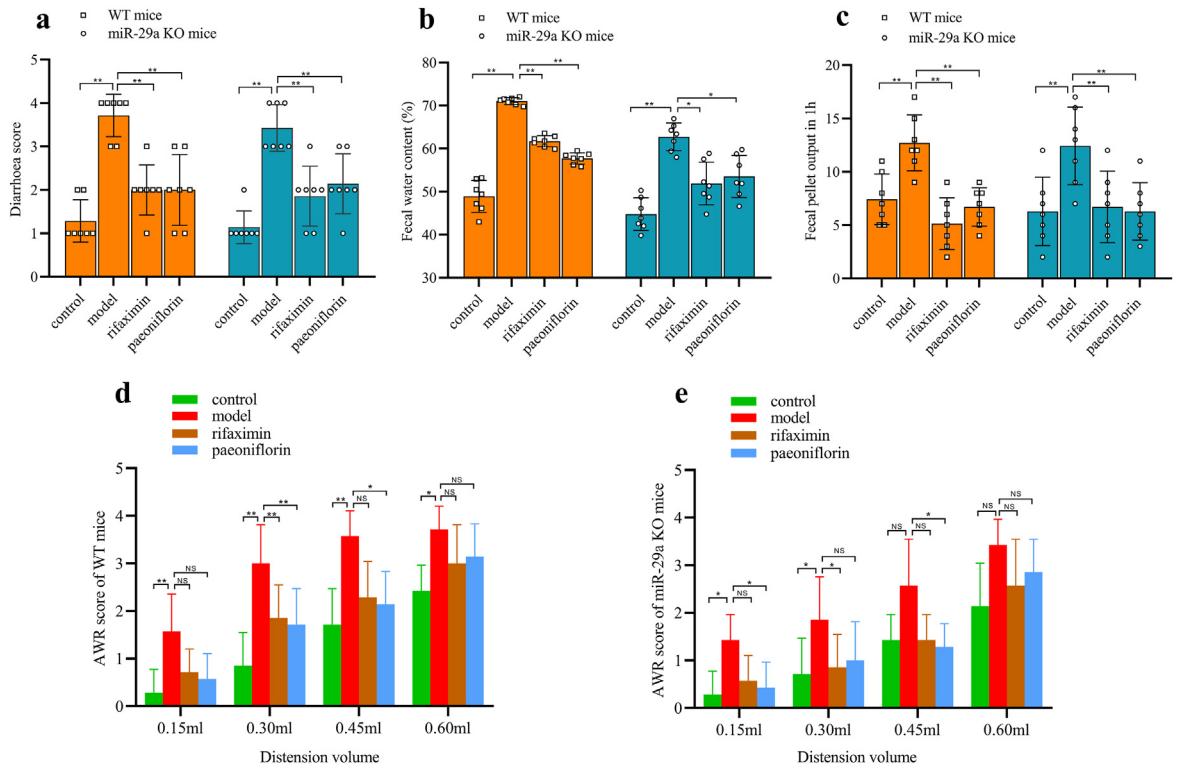

Figure 1. Paeoniflorin treatment alleviates the main symptoms of IBS-D. (a) diarrhea score, (b) fecal water content, (c) fecal pellet output, (d, e) abdominal withdrawal reflex (AWR) scores. Results are presented as mean ± SD, n = 7. (*$P < 0.05$; **$P < 0.01$; NS, no significance).

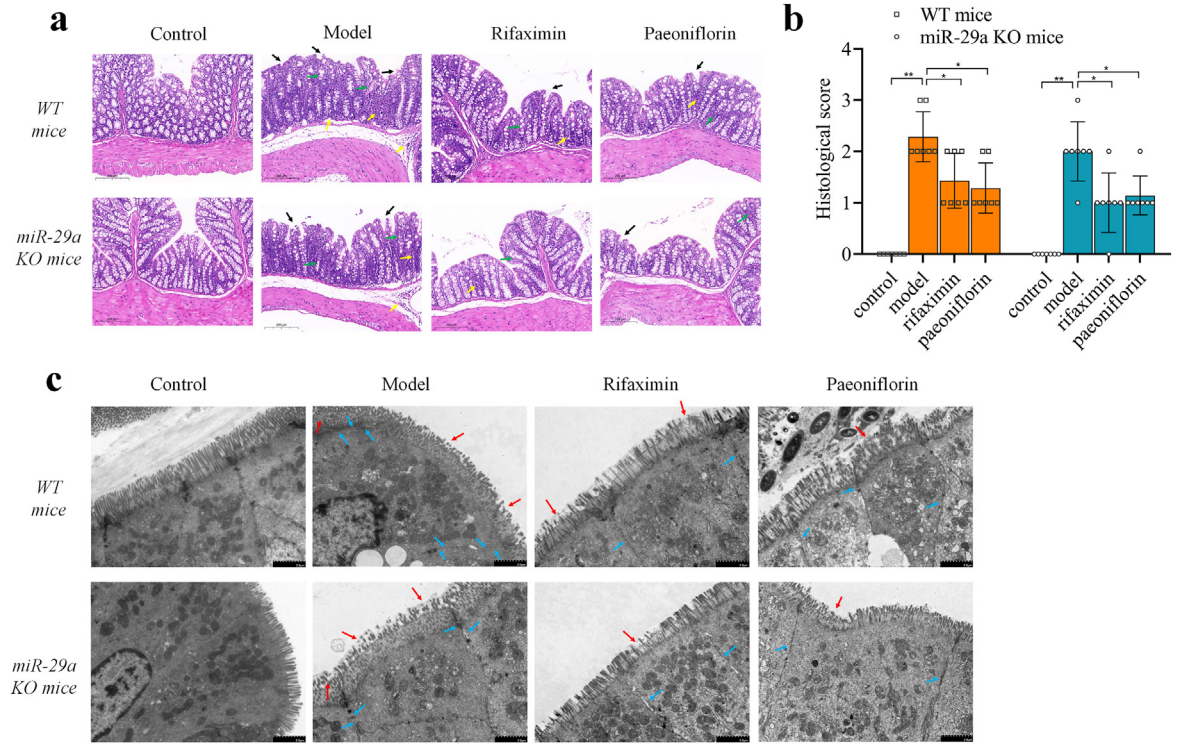

Figure 2. Paeoniflorin treatment remediates mouse colon tissue damage. (a) Changes in colon tissue structure: black arrows indicate loss of tissue structure, green arrows indicate damage to mucosal glands and edema, and yellow arrows indicate inflammatory cell infiltration (scale bars 200 μm). (b) Histological score. Results are presented as mean ± SD, n = 7. (*$P < 0.05$; **$P < 0.01$; NS, no significance). (c) TEM images: red arrows indicate sparsely arranged microvilli with uneven distribution and different lengths, and blue arrows indicate light staining and discontinuous junctional complex (scale bars 2 μm).

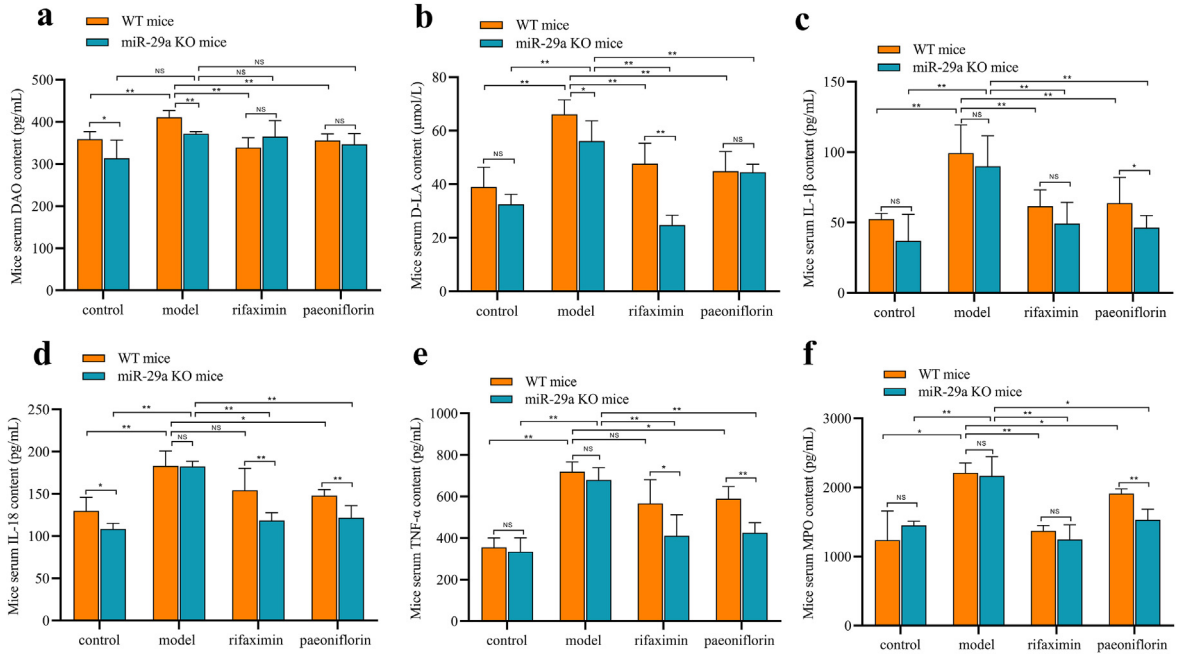

Figure 3. Changes in serum levels of (a) DAO, (b) D-LA, (c) IL-1β, (d) IL-18, (e) TNF-α, and (f) MPO. Results are presented as mean ± SD, n = 7. (*$P < 0.05$; **$P < 0.01$; NS, no significance).

Additionally, serum IL-1β levels were decreased in the rifaximin or paeoniflorin groups compared to those in the IBS-D group (both $P < 0.01$) (Figure 3c). Moreover, serum IL-1β levels were lower in miR-29a KO mice than in WT mice in the paeoniflorin group ($P < 0.05$) (Figure 3c). However, serum IL-1β levels did not differ between WT and miR-29a KO mice among the corresponding control, IBS-D model, and rifaximin groups ($P > 0.05$) (Figure 3c).

For both WT and miR-29a KO mice, serum IL-18 levels were higher in the IBS-D model group than in the control group ($P < 0.01$) (Figure 3d). Additionally, serum IL-18 levels in the paeoniflorin group were lower than those in the model group for WT mice (both $P < 0.05$) (Figure 3d). Meanwhile, serum IL-18 levels in the rifaximin group did not differ from those in the IBS-D model group ($P > 0.05$). For miR-29a KO mice, serum IL-18 levels in the rifaximin and paeoniflorin groups were lower than those in the IBS-D model group (both P < 0.01) (Figure 3d). Serum IL-18 levels were decreased in miR-29a KO mice in the control, rifaximin and paeoniflorin group compared to corresponding groups in WT mice ($P < 0.05$) (Figure 3d). However, serum IL-18 levels did not differ between WT and miR-29a KO mice among IBS-D model group (P > 0.05) (Figure 3d).

For both WT and miR-29a KO mice, serum TNF-α levels were higher in the IBS-D model group than in the control group ($P < 0.01$). Additionally, serum TNF-α levels were lower in the paeoniflorin group than in the IBS-D model group for WT mice ($P < 0.01$) (Figure 3e). Meanwhile, serum TNF-α levels in the rifaximin group did not differ from those in the IBS-D model group (P > 0.05). For miR-29a KO mice, TNF-α levels in the rifaximin and paeoniflorin groups were lower than those in the IBS-D model group (both P < 0.01) (Figure 3e). In the rifaximin and paeoniflorin groups, serum TNF-α levels were lower in miR-29a KO mice than in WT mice ($P < 0.01$) (Figure 3e). However, serum TNF-α levels did not differ between WT and miR-29a KO mice among the corresponding control, IBS-D model groups (P > 0.05) (Figure 3e).

For both WT and miR-29a KO mice, the IBS-D model group had higher serum MPO levels than the control group ($P < 0.05$ or $P < 0.01$) (Figure 3f). Additionally, serum MPO levels were decreased in the rifaximin ($P < 0.01$) and paeoniflorin groups ($P < 0.05$) compared to those in the IBS-D model group (Figure 3f). Moreover, serum MPO levels in miR-29a KO mice were lower than those in WT mice in the paeoniflorin group ($P < 0.01$). However, serum MPO levels did not differ between WT and miR-29a KO mice among the corresponding control, IBS-D model, and rifaximin groups ($P > 0.05$) (Figure 3f).

3.4. *miR-29a can target NKRF and indirectly modulate NLRP3 inflammasomes*

Target analysis and the dual-luciferase reporter gene assay were performed to determine whether miR-29a can regulate NKRF. Online miRNA target analysis suggested a binding site between miR-29a-3p and the NKRF 3′ UTR (Figure 4a), which was further verified by the results of the dual-luciferase reporter assay (Figure 4b). The luciferase activity of the miR-29a-3p mimic was lower than that of the mimic control WT-NKRF 3′ UTR, which was not significantly different from that of the mutated NKRF 3' UTR vector (Figure 4b). These results confirmed a potential negative regulatory effect of miR-29a-3p on NKRF expression.

As previous study reported that NF-κB is a key factor for priming NLRP3 inflammasome activation [21] and NKRF was shown to be a direct target of miR-29a in IBS-D [20]. Taken together, the results suggest that inflammasome activation and expression of NLRP3 could be indirectly regulated by miR-29a, with NF-κB being closely involved.

3.5. *Expression of miR-29a and NKRF, NF-κB (p65), NLRP3, ASC, caspase-1, IL-1β and TNF-α mRNA in mouse colon tissues*

In WT mice, miR-29a expression was upregulated in the IBS-D model group compared to that in the control group ($P < 0.01$). Moreover, miR-29a expression was significantly lower in the rifaximin and paeoniflorin groups (both $P < 0.01$) than in the IBS-D model group (Figure 5a). In miR-29a KO mice, miR-29a expression did not differ among the groups ($P > 0.05$) (Figure 5a). Additionally, miR-29a expression was lower in miR-29a KO mice than in WT mice among the corresponding groups ($P_{all} < 0.01$) (Figure 5a).

For WT and miR-29a KO mice, NKRF mRNA expression was decreased in the IBS-D model group compared to that in the control group ($P < 0.01$). Additionally, NKRF mRNA expression was significantly elevated in the rifaximin and paeoniflorin groups compared to that in the IBS-D model group ($P < 0.01$) (Figure 5b). Moreover, NKRF mRNA

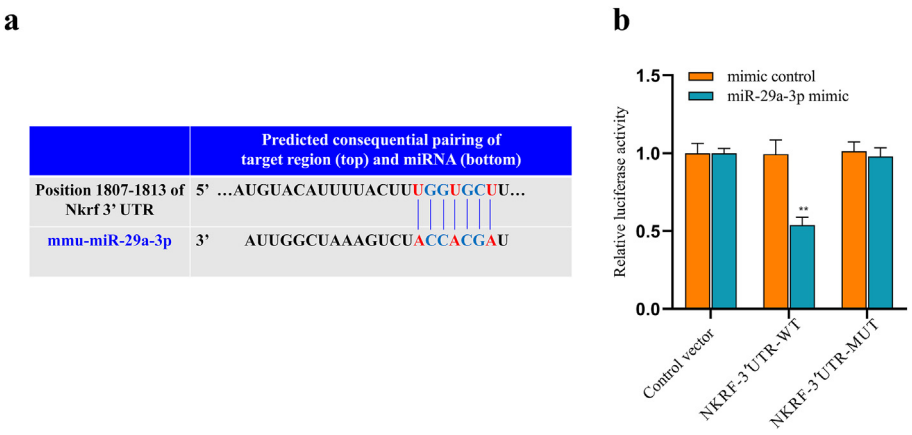

Figure 4. Target analysis and dual-luciferase reporter gene assay confirming that miR-29a can regulate NKRF. (a) Binding site between miR-29a-3p and NKRF 3′ UTR. (b) Results of dual-luciferase reporter assay. Results are presented as mean ± SD, n = 5. (**$P < 0.01$ vs. mimic control).

expression was higher in miR-29a KO mice than in WT mice among the corresponding control, rifaximin, and paeoniflorin groups ($P < 0.01$) (Figure 5b). However, no significant difference in NKRF mRNA expression was found between WT and miR-29a KO mice in the IBS-D model group ($P > 0.05$) (Figure 5b).

For WT and miR-29a KO mice, NF-κB (p65) mRNA expression was higher in the IBS-D model group than in the control group ($P < 0.01$ or $P < 0.05$) (Figure 5c). Additionally, NF-κB (p65) mRNA expression was decreased in the rifaximin and paeoniflorin groups compared to that in the IBS-D model group for WT mice ($P < 0.01$) (Figure 5c). For miR-29a KO mice, NF-κB (p65) mRNA expression in the rifaximin and paeoniflorin groups was lower than that in IBS-D model group (both $P < 0.05$) (Figure 5c). Moreover, NF-κB (p65) mRNA expression in the IBS-D model, rifaximin and paeoniflorin groups was decreased in miR-29a KO mice compared to that in WT mice ($P_{all} < 0.01$) (Figure 5c). However, NF-κB (p65) mRNA expression did not differ between WT and miR-29a KO mice in the control groups (P > 0.05) (Figure 5c).

For WT and miR-29a KO mice, NLRP3 mRNA expression was higher in the IBS-D model group than in the control group ($P < 0.01$ or $P < 0.05$). Additionally, NLRP3 mRNA expression was downregulated in the rifaximin and paeoniflorin groups compared to that in the IBS-D model group for WT mice ($P_{rifaximin}<0.01$, $P_{paeoniflorin}<0.05$) (Figure 5d). However, NLRP3 mRNA expression did not differ in the rifaximin and paeoniflorin groups compared to that in the IBS-D model group for miR-29a KO mice ($P > 0.05$) (Figure 5d). Moreover, NLRP3 mRNA expression was lower in miR-29a KO mice than in WT mice in the IBS-D model and paeoniflorin group ($P_{all} < 0.05$) (Figure 5d). However, NLRP3 mRNA expression did not differ between WT and miR-29a KO mice among the corresponding control and rifaximin groups ($P > 0.05$) (Figure 5d).

For WT and miR-29a KO mice, ASC mRNA expression was higher in the IBS-D model group than in the control group (P < 0.01 or P < 0.05) (Figure 5e). Additionally, ASC mRNA expression was significantly decreased in the rifaximin and paeoniflorin groups compared to that in the IBS-D model group ($P_{rifaximin}<0.01$, $P_{paeoniflorin}<0.05$) (Figure 5e). Moreover, ASC mRNA expression was lower in miR-29a KO mice than in WT mice of all the corresponding groups ($P_{all} < 0.05$) (Figure 5e).

For WT and miR-29a KO mice, caspase-1 mRNA expression was increased in the IBS-D model group compared to that in the control group ($P < 0.01$ or $P < 0.05$) (Figure 5f). Additionally, caspase-1 mRNA expression was significantly decreased in the rifaximin and paeoniflorin groups compared to that in the IBS-D model group ($P < 0.01$) (Figure 5f). Moreover, caspase-1 mRNA expression was lower in miR-29a KO mice than in WT mice among all the corresponding groups ($P_{all} < 0.05$) (Figure 5f).

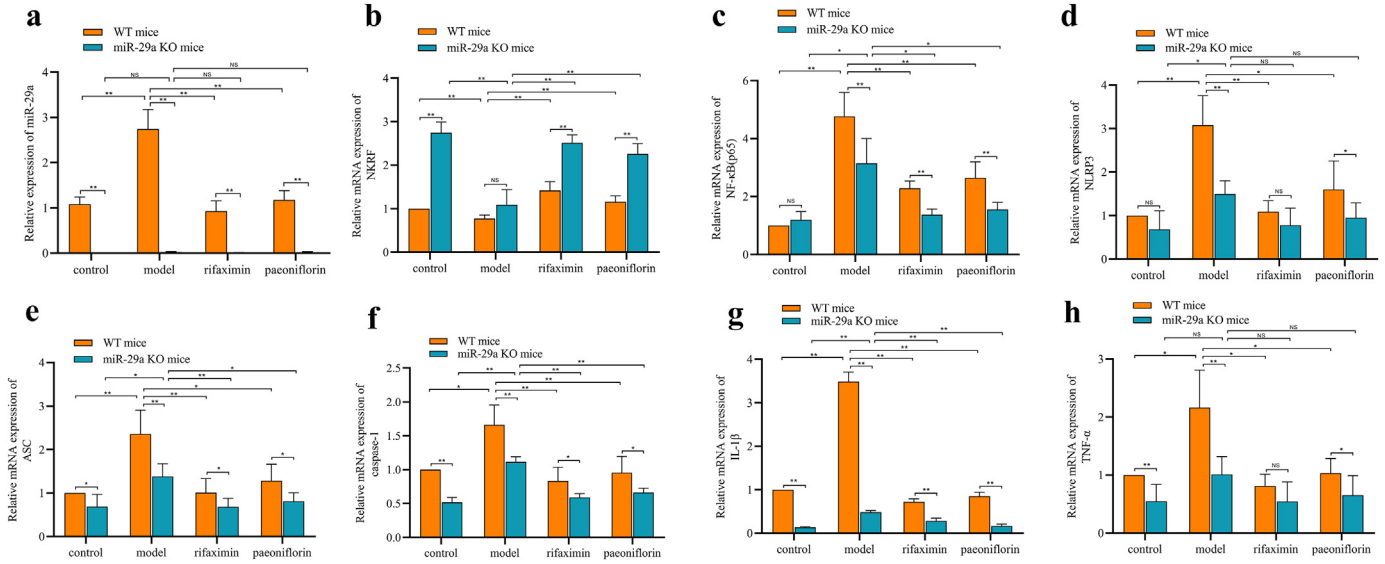

Figure 5. RT-qPCR analysis of (a) miR-29a, (b) NKRF mRNA, (c) NF-κB (p65) mRNA, (d) NLRP3 mRNA, (e) ASC mRNA, (f) caspase-1 mRNA, (g) IL-1β mRNA, and (h) TNF-α mRNA expression in mouse colon tissues. Results are presented as mean ± SD, n = 7. (*$P < 0.05$; **$P < 0.01$; NS, no significance).

For WT and miR-29a KO mice, IL-1β mRNA expression was upregulated in the IBS-D model group compared to that in the control group ($P < 0.01$) (Figure 5g). Additionally, IL-1β mRNA expression was decreased in the rifaximin and paeoniflorin groups compared to that in the IBS-D model group ($P < 0.01$) (Figure 5g). Moreover, IL-1β mRNA expression was lower in miR-29a KO mice than in WT mice among the corresponding groups ($P_{all} < 0.01$) (Figure 5g).

For WT mice, TNF-α mRNA expression was upregulated in the IBS-D model group compared to that in the control group ($P < 0.05$) (Figure 5h). Additionally, TNF-α mRNA expression was significantly decreased in the rifaximin and paeoniflorin groups compared to that in the IBS-D model group (both $P < 0.05$) (Figure 5h). However, TNF-α mRNA expression did not differ significantly in miR-29a KO mice among the groups ($P > 0.05$) (Figure 5h). Compared to that in WT mice in the IBS-D model group, TNF-α mRNA expression was downregulated in miR-29a KO mice in the control, IBS-D model and paeoniflorin groups ($P_{all} < 0.05$) (Figure 5h). However, TNF-α mRNA expression did not differ between WT and miR-29a KO mice among the rifaximin groups ($P > 0.05$) (Figure 5h).

3.6. Immunohistochemical localization of NLRP3, ASC, and caspase-1 in mouse colon tissues

For both WT and miR-29a KO mice, NLRP3 protein expression was upregulated in the IBS-D model group compared to that in the corresponding control, rifaximin, and paeoniflorin groups ($P_{all} < 0.01$) (Figure 6a, d). Moreover, NLRP3 protein expression was downregulated in miR-29a KO mice compared to that in WT mice among the corresponding control, IBS-D model, and paeoniflorin groups ($P_{control}<0.01$, $P_{model}<0.05$, $P_{paeoniflorin}<0.05$) (Figure 6a, d). However, NLRP3 protein expression did not differ between WT and miR-29a KO mice in the rifaximin group ($P > 0.05$) (Figure 6a, d).

For both WT and miR-29a KO mice, ASC protein expression was upregulated in the IBS-D model group compared to that in the control group ($P_{all} < 0.01$) (Figure 6b, e). Additionally, ASC protein expression was downregulated in the rifaximin and paeoniflorin groups compared to that in the IBS-D model group (both $P < 0.01$) (Figure 6b, e). Moreover, ASC protein expression was downregulated in miR-29a KO mice compared to that in WT mice among the corresponding control, IBS-D model, and paeoniflorin groups ($P_{all} < 0.01$) (Figure 6b, e). However, ASC protein expression did not differ between WT and miR-29a KO mice in the rifaximin group ($P > 0.05$) (Figure 6b, e).

For both WT and miR-29a KO mice, caspase-1 protein expression was upregulated in the IBS-D model group compared to that in the control group (both $P < 0.01$) (Figure 6c, f). Additionally, caspase-1 protein expression was significantly decreased in the rifaximin group compared to that in the IBS-D model ($P_{WT}<0.05$, $P_{miR\text{-}29a\ KO}<0.01$) and paeoniflorin groups (both $P < 0.01$) (Figure 6c, f). Compared to that in WT mice, caspase-1 protein expression in miR-29a KO mice was downregulated in the rifaximin and paeoniflorin groups ($P < 0.05$) (Figure 6c, f). However, caspase-1 protein expression did not differ between WT and miR-29a KO mice among the corresponding control, IBS-D model groups ($P_{all} > 0.05$) (Figure 6c, f).

3.7. Immunohistochemical localization of claudin-1 and ZO-1 in mouse colon tissues

For both WT and miR-29a KO mice, claudin-1 protein expression was decreased in the IBS-D model group compared to that in the control group ($P < 0.01$) (Figure 7a, c). Additionally, claudin-1 protein expression was increased in the rifaximin and paeoniflorin groups compared to that in the IBS-D model group ($P_{all} < 0.01$) (Figure 7a, c). Moreover, claudin-1 protein expression did not differ between WT and miR-29a KO mice among the corresponding groups ($P_{all} > 0.05$) (Figure 7a, c).

For WT mice, ZO-1 protein expression was downregulated in the IBS-D model group compared to that in the control group ($P < 0.01$) (Figure 7b, d). Additionally, ZO-1 protein expression was increased in the rifaximin ($P_{WT}<0.01$, $P_{miR\text{-}29a\ KO}<0.05$) and paeoniflorin groups ($P_{WT}<0.05$, $P_{miR\text{-}29a\ KO}<0.01$) compared to that in the IBS-D model group (Figure 7b, d). Moreover, ZO-1 protein expression was downregulated in miR-29a KO mice compared to that in WT mice in the control group ($P < 0.05$) (Figure 7b, d). However, ZO-1 protein expression did not differ between WT and miR-29a mice among the corresponding IBS-D model, rifaximin, and paeoniflorin groups ($P_{all} > 0.05$) (Figure 7b, d).

4. Discussion

The current study aimed to evaluate the efficacy of paeoniflorin, the main active ingredient in the traditional Chinese medicine *P. lactiflora* Pall., in modulating the intestinal immune response in an IBS-D mouse model and elucidate the underlying mechanism. The results indicated that paeoniflorin exerted protective effects by decreasing the expression of miR-29a, NF-κB (p65), NLRP3, ASC, caspase-1, IL-1β, and TNF-α in the colon tissues of IBS-D model mice while increasing the expression of NKRF, ZO-1, and claudin-1.

Researchers have reported that psychological or physical comorbidity is common in patients with IBS-D [39, 40]. Stress can result in increased frequency of intestinal transit, which limits water absorption by excrement, leading to liquid stool [41]. In the current study, the mean diarrhea scores and fecal water content for both mouse lineages were significantly increased in the IBS-D model group, which was consistent with the observation of watery stool excreted by the IBS-D model mice. Paeoniflorin treatment resulted in decreased diarrhea scores and fecal water content, as well as firmer stool, suggesting that paeoniflorin effectively improved diarrheal symptoms in IBS-D. Fecal pellet output during 1 h of restraint stress was higher in the IBS-D model group than in the control group, suggesting elevated colonic motility under stress conditions. However, stool frequency decreased significantly after paeoniflorin treatment, suggesting that paeoniflorin alleviated hyperactive intestinal motility function. Consistent with the diarrhea score and bowel frequency results, paeoniflorin treatment significantly reduced visceral hypersensitivity in IBS-D model mice, which is considered to be a critical factor in the pathogenesis of IBS-D [42]. The higher fecal pellet output aligned with higher AWR scores, since colorectal hypersensitivity and fecal urgency are correlated with diarrhea [37]. Intestinal inflammation, which is involved in colonic mucosa damage, polymorphonuclear neutrophil infiltration, and mucosal gland impairment, is prevalent in patients with IBS-D [11]. Histological analysis in the current study demonstrated that mucosal gland damage, edema, and inflammatory cell infiltration were more severe in the IBS-D model group than in the control group and were ameliorated by paeoniflorin treatment. Moreover, paeoniflorin treatment remarkably downregulated serum MPO levels, a marker of neutrophil infiltration [43], in both mouse lineages. Plasma DAO and D-LA levels are useful markers for assessing intestinal permeability [44, 45]. Paeoniflorin treatment reduced serum DAO and D-LA concentrations in IBS-D model mice, with much lower levels in miR-29a KO mice than in WT mice, indicating that paeoniflorin improved intestinal barrier dysfunction. Finally, the TEM images revealed that paeoniflorin treatment ameliorated or restored the widened junctional complexes, damaged intestinal epithelial cells, and scattered microvilli to varying degrees.

Interestingly, the diarrhea score, fecal pellet output, and histological score did not differ significantly between WT and miR-29a KO mice in the IBS-D model group. The results suggest that knocking out miR-29a alone may not have caused significant differences in some of the macroscopic pathological manifestations of IBS-D between WT and miR-29a KO mice, especially those graded semi-quantitatively, such as diarrhea and histological scores. Nevertheless, paeoniflorin treatment induced therapeutic effects in IBS-D model mice for both mouse lineages, as judged by the diarrhea and histological scores.

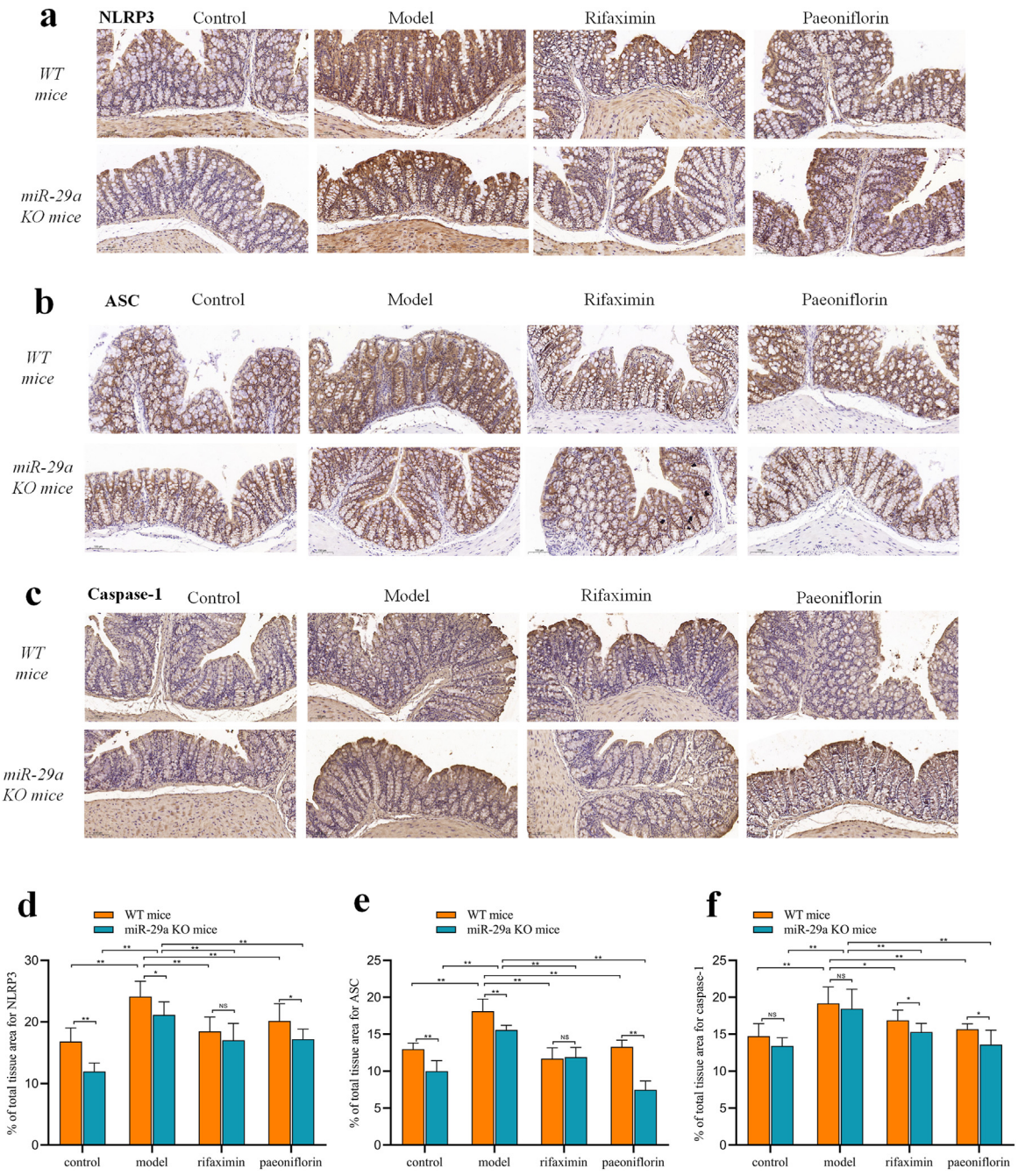

Figure 6. Immunohistochemical analysis of NLRP3, ASC, and caspase-1 in mouse colon tissues. Representative images of (a) NLRP3 protein expression, (b) ASC protein expression, and (c) caspase-1 protein expression. Quantification of total tissue area stained for (d) NLRP3, (e) ASC, and (f) caspase-1. Results are presented as mean ± SD, n = 7. (*$P < 0.05$; **$P < 0.01$; NS, no significance).

Inflammasomes can regulate the innate immune response by activating ASC and caspase-1 and producing IL-1β and IL-18 during intestinal inflammation [10, 46]. By participating in the management of gut microbiota and intestinal homeostasis, NLRP3 seems to be deeply involved in IBS-D pathophysiology [47, 48]. The RT-qPCR results in the current study indicated that paeoniflorin treatment significantly decreased the expression of NF-κB (p65), NLRP3, ASC, caspase-1, and IL-1β in IBS-D model mice, while increasing NKRF expression. Interestingly, the expression of NLRP3 pathway targets was generally lower in miR-29a KO mice than in WT mice. Combined with the dual-luciferase assay results indicating that miR-29a can directly bind to the NKRF 3' UTR and decrease NLRP3 expression, the results suggest that paeoniflorin may inhibit the NLRP3 inflammasome pathway by downregulating miR-29a expression. A previous study reported that NF-κB is a key factor for priming NLRP3 inflammasome activation [21] and NKRF was shown to be a direct target of miR-29a in IBS-D [20]. Taken together, the results suggest that inflammasome activation and expression of NLRP3 could be indirectly regulated by miR-29a, with NF-κB being closely involved.

As a downstream target of the NLRP3 pathway, serum IL-18 levels did not differ between WT and miR-29a KO mice in the IBS-D model group, but differed significantly after paeoniflorin treatment. This result suggests that downregulation of IL-18 was induced by paeoniflorin treatment and was not the consequence of miR-29a knockout. Further, serum IL-18

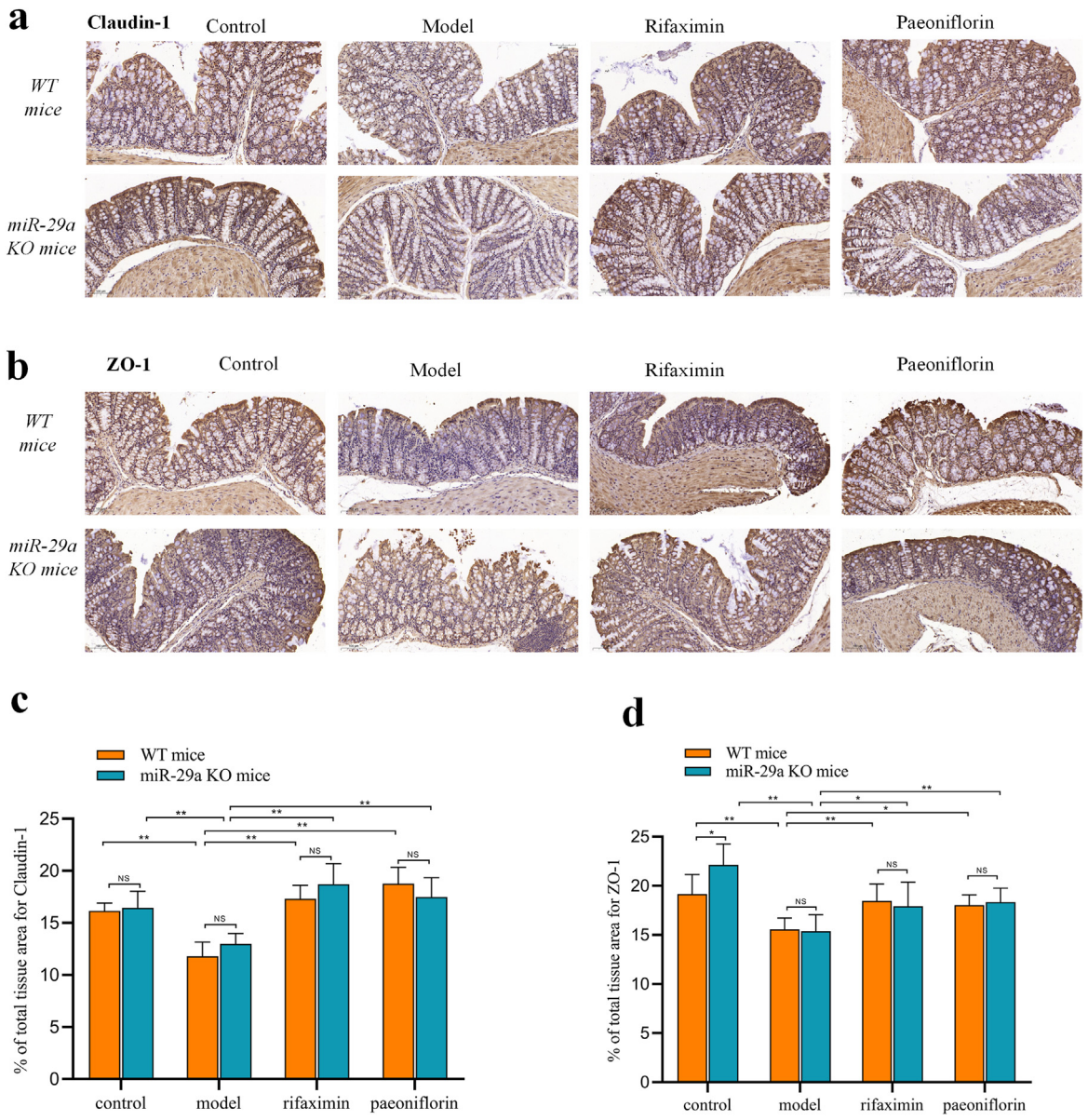

Figure 7. Immunohistochemical analysis of claudin-1 and ZO-1 in mouse colon tissues. Representative images of (a) claudin-1 protein expression and (b) ZO-1 protein expression. Quantification of total tissue area stained for (c) claudin-1 and (d) ZO-1. Results are presented as mean ± SD, n = 7. (*$P < 0.05$; **$P < 0.01$; NS, no significance).

levels were lower in miR-29a KO mice than in WT mice after paeoniflorin treatment, supporting that miR-29a knockout helped alleviate the inflammasome response. Similar to the IL-18 results, TNF-α expression did not differ between the two mouse lineages in the IBS-D model group and was differentially downregulated after paeoniflorin treatment. Activation of the NF-κB pathway in the intestine promotes NLRP3 expression, which in turn enhances the expression of IL-1β and TNF-α [21, 49]. Thus, similar results were expected for IL-1β and TNF-α. However, TNF-α mRNA expression (Figure 5h) in mouse colon tissues did not align with the serum profile. Paeoniflorin may inhibit the expression of inflammatory targets (including TNF-α) via downregulation of miR-29a. Therefore, miR-29a knockout weakened the effectiveness of paeoniflorin by downregulating TNF-α expression, resulting in comparable TNF-α levels in miR-29a KO mice. Nevertheless, NLRP3, ASC, and caspase-1 protein levels in the colon tissues of WT mice were significantly higher than those in the colon tissues of miR-29a KO mice (Figure 6), suggesting that paeoniflorin inhibited NLRP3 inflammasome activation, thus providing further support for the role of miR-29a in this cascade mechanism (Figure 8).

Claudin-1 and ZO-1 are tight junction proteins needed for physiological epithelial barrier function and to maintain intestinal permeability [50]. Disruption of the intestinal epithelial barrier can increase intestinal permeability, resulting in the transfer of pathogens and allergens from the lumen into blood circulation, destruction of immune homeostasis, and activation of the intestinal inflammatory response [51, 52, 53]. The IHC results revealed that claudin-1 and ZO-1 expression was lower in the colon tissues of both mouse lineages in the IBS-D model group and was enhanced after paeoniflorin treatment. These results suggest that paeoniflorin treatment may restore the damaged colonic epithelium in IBS-D model mice by upregulating the expression of tight junction proteins, which concurs with previously reported results that paeoniflorin inhibited the destruction of tight junction proteins induced by lipopolysaccharide stimulation in Caco-2 cells [26]. Nevertheless, claudin-1 and ZO-1 protein levels did not differ significantly between WT and miR-29a KO mice among corresponding groups, suggesting the possible involvement of multiple miRNAs in the regulation of intestinal tight junction proteins in IBS-D, including miR-200C-3p, miR-16, and miR-125b [54,55]. Thus,

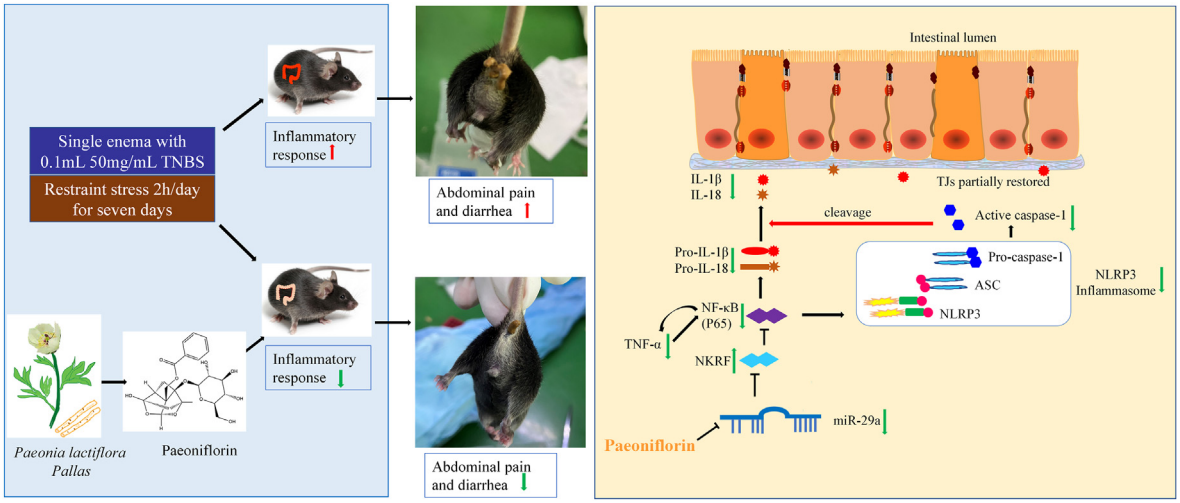

Figure 8. Diagram of pharmacological mechanism of paeoniflorin on IBS-D. Paeoniflorin alleviates the inflammatory response of IBS-D by downregulating miR-29a expression and inhibiting the abnormal activation of the NLRP3 inflammasome pathway with NF-κB being closely involved.

knocking out miR-29a alone may not have resulted in significant differences in claudin-1 and ZO-1 expression if other miRNAs can exert compensatory functions in tight junction protein expression.

5. Conclusions

In conclusion, the study findings suggest that paeoniflorin alleviates the inflammatory response in IBS-D by downregulating miR-29a expression and inhibiting abnormal activation of the NLRP3 inflammasome pathway, thereby restraining the proinflammatory response of the intestinal mucosa and promoting recovery of the intestinal epithelial barrier. The role of miR-29a in IBS-D and molecular mechanisms underlying the pharmacological effects of paeoniflorin on intestinal tract disorder warrant further exploration. Nevertheless, together with previously reported findings, the results of the current study indicate that paeoniflorin serves as a promising candidate for the treatment of IBS-D symptoms associated with inflammatory reactions.

Declarations

Author contribution statement

Wei Ke; Yongfu Wang; Hongmei Tang: Conceived and designed the experiments; Analyzed and interpreted the data; Wrote the paper.

Siyu Huang; Shan Liu; He Zhu; Xiangyu Xie; Huifei Yang: Performed the experiments.

Qin Lu; Jianfeng Gan; Guodong He; Fei Che; Xin Wan: Contributed reagents, materials, analysis tools or data.

Funding statement

This work was supported by the following three funding programs: 1. the National Natural Science Foundation of China, China (grant no. 81673842); 2. Natural Science Foundation of Guangdong Province, China (grant no. 2019A1515011745); 3. Natural Science Foundation of Guangdong Province, China (grant no. 2021A1515110727).

Data availability statement

Data will be made available on request.

Declaration of interest's statement

The authors declare no competing interests.

Additional information

Supplementary content related to this article has been published online at https://doi.org/10.1016/j.heliyon.2022.e12312.

References

[1] F. Mearin, B.E. Lacy, L. Chang, et al., Bowel disorders, Gastroenterology S0016-5085 (16) (2016) 222–225.
[2] P. Oka, H. Parr, B. Barberio, et al., Global prevalence of irritable bowel syndrome according to Rome III or IV criteria: a systematic review and meta-analysis, Lancet Gastroenterol. Hepatol. 5 (10) (2020) 908–917.
[3] C. Canavan, J. West, T. Card, Review article: the economic impact of the irritable bowel syndrome, Aliment. Pharmacol. Ther. 40 (9) (2014) 1023–1034.
[4] D.A. Drossman, Functional gastrointestinal disorders: history, pathophysiology, clinical features and Rome IV, Gastroenterology S0016-5085 (16) (2016) 223–227.
[5] J.M. Harvey, A. Sibelli, T. Chalder, et al., Desperately seeking a cure: treatment seeking and appraisal in irritable bowel syndrome, Br. J. Health Psychol. 23 (3) (2018) 561–579.
[6] N.J. Talley, What causes functional gastrointestinal disorders? A proposed disease model, Am. J. Gastroenterol. 115 (1) (2020) 41–48.
[7] J.J. Martin-Vinas, E.M. Quigley, Immune response in irritable bowel syndrome: a systematic review of systemic and mucosal inflammatory mediators, J Dig Dis 17 (9) (2016) 572–581.
[8] M. Bashashati, S. Moossavi, C. Cremon, et al., Colonic immune cells in irritable bowel syndrome: a systematic review and meta-analysis, Neuro Gastroenterol. Motil. 30 (1) (2018).
[9] L. Ohman, M. Simren, Pathogenesis of IBS: role of inflammation, immunity and neuroimmune interactions, Nat. Rev. Gastroenterol. Hepatol. 7 (3) (2010) 163–173.
[10] Y. Zhen, H. Zhang, NLRP3 inflammasome and inflammatory bowel disease, Front. Immunol. 10 (2019) 276.
[11] S.A. Scuderi, G. Casili, M. Lanza, et al., Modulation of NLRP3 inflammasome attenuated inflammatory response associated to diarrhea-predominant irritable bowel syndrome, Biomedicines 8 (11) (2020).
[12] S.K. Vanaja, V.A. Rathinam, K.A. Fitzgerald, Mechanisms of inflammasome activation: recent advances and novel insights, Trends Cell Biol. 25 (5) (2015) 308–315.
[13] L. de Almeida, S. Khare, A.V. Misharin, et al., The PYRIN domain-only protein POP1 inhibits inflammasome assembly and ameliorates inflammatory disease, Immunity 43 (2) (2015) 264–276.
[14] G. Barbara, M.R. Barbaro, D. Fuschi, et al., Inflammatory and microbiota-related regulation of the intestinal epithelial barrier, Front. Nutr. 8 (2021), 718356.
[15] J. Matricon, M. Meleine, A. Gelot, et al., Review article: associations between immune activation, intestinal permeability and the irritable bowel syndrome, Aliment. Pharmacol. Ther. 36 (11-12) (2012) 1009–1031.
[16] M. Pimentel, A. Lembo, W.D. Chey, et al., Rifaximin therapy for patients with irritable bowel syndrome without constipation, N. Engl. J. Med. 364 (1) (2011) 22–32.
[17] D. Xu, J. Gao, M. Gillilland 3rd, et al., Rifaximin alters intestinal bacteria and prevents stress-induced gut inflammation and visceral hyperalgesia in rats, Gastroenterology 146 (2) (2014) 484–496 e4.
[18] T.X. Lu, M.E. Rothenberg, MicroRNA, J. Allergy Clin. Immunol. 141 (4) (2018) 1202–1207.
[19] Q. Zhou, W.W. Souba, C.M. Croce, et al., MicroRNA-29a regulates intestinal membrane permeability in patients with irritable bowel syndrome, Gut 59 (6) (2010) 775–784.
[20] Q. Zhou, S. Costinean, C.M. Croce, et al., MicroRNA 29 targets nuclear factor-kappaB-repressing factor and Claudin 1 to increase intestinal permeability, Gastroenterology 148 (1) (2015) 158–169 e8.

[21] F.G. Bauernfeind, G. Horvath, A. Stutz, et al., Cutting edge: NF-kappaB activating pattern recognition and cytokine receptors license NLRP3 inflammasome activation by regulating NLRP3 expression, J. Immunol. 183 (2) (2009) 787–791.
[22] M. Chen, T.C. Tang, Y. Wang, et al., Randomised clinical trial: Tong-Xie-Yao-Fang granules versus placebo for patients with diarrhoea-predominant irritable bowel syndrome, Aliment. Pharmacol. Ther. 48 (2) (2018) 160–168.
[23] G. Wang, T.Q. Li, L. Wang, et al., Tong-xie-ning, a Chinese herbal formula, in treatment of diarrhea-predominant irritable bowel syndrome: a prospective, randomized, double-blind, placebo-controlled trial, Chin. Med. J. (Engl.). 119 (24) (2006) 2114–2119. PMID: 17199964.
[24] X. Luo, X. Wang, S. Huang, et al., Paeoniflorin ameliorates experimental colitis by inhibiting gram-positive bacteria-dependent MDP-NOD2 pathway, Int. Immunopharm. 90 (2021), 107224.
[25] Q. Fan, X. Guan, Y. Hou, et al., Paeoniflorin modulates gut microbial production of indole-3-lactate and epithelial autophagy to alleviate colitis in mice, Phytomedicine 79 (2020), 153345.
[26] X.X. Wu, X.L. Huang, R.R. Chen, et al., Paeoniflorin prevents intestinal barrier disruption and inhibits lipopolysaccharide (LPS)-Induced inflammation in Caco-2 cell monolayers, Inflammation 42 (6) (2019) 2215–2225.
[27] X.J. Zhang, Z. Li, W.M. Leung, et al., The analgesic effect of paeoniflorin on neonatal maternal separation-induced visceral hyperalgesia in rats, J. Pain 9 (6) (2008) 497–505.
[28] H. Zhu, X. Xiao, Y. Chai, et al., MiRNA-29a modulates visceral hyperalgesia in irritable bowel syndrome by targeting HTR7, Biochem. Biophys. Res. Commun. 511 (3) (2019) 671–678.
[29] C.L. Williams, R.G. Villar, J.M. Peterson, et al., Stress-induced changes in intestinal transit in the rat: a model for irritable bowel syndrome, Gastroenterology 94 (3) (1988) 611–621.
[30] D.J. Kang, G. Kakiyama, N.S. Betrapally, et al., Rifaximin exerts beneficial effects independent of its ability to alter microbiota composition, Clin. Transl. Gastroenterol. 7 (8) (2016) e187.
[31] J. Zhang, W. Dou, E. Zhang, et al., Paeoniflorin abrogates DSS-induced colitis via a TLR4-dependent pathway, Am. J. Physiol. Gastrointest. Liver Physiol. 306 (1) (2014) G27–36.
[32] J. Aguilera-Lizarraga, M.V. Florens, M.F. Viola, et al., Local immune response to food antigens drives meal-induced abdominal pain, Nature 590 (7844) (2021) 151–156.
[33] E.D. Al-Chaer, M. Kawasaki, P.J. Pasricha, A new model of chronic visceral hypersensitivity in adult rats induced by colon irritation during postnatal development, Gastroenterology 119 (5) (2000) 1276–1285.
[34] C. Asseman, S. Mauze, M.W. Leach, et al., An essential role for interleukin 10 in the function of regulatory T cells that inhibit intestinal inflammation, J. Exp. Med. 190 (7) (1999) 995–1004.
[35] F. Zhang, W. Wang, J. Niu, et al., Heat-shock transcription factor 2 promotes sodium butyrate-induced autophagy by inhibiting mTOR in ulcerative colitis, Exp. Cell Res. 388 (1) (2020), 111820.
[36] E. Esposito, D. Impellizzeri, E. Mazzon, et al., Neuroprotective activities of palmitoylethanolamide in an animal model of Parkinson's disease, PLoS One 7 (8) (2012), e41880.
[37] V. Rangan, J. Nee, P. Singh, et al., Fecal urgency: clinical and manometric characteristics in patients with and without diarrhea, Dig. Dis. Sci. 65 (12) (2020) 3679–3687.
[38] H. Shamshiri, P. Paragomi, M.J. Paydar, et al., Antinociceptive effect of chronic lithium on visceral hypersensitivity in a rat model of diarrhea-predominant irritable bowel syndrome: the role of nitric oxide pathway, J. Gastroenterol. Hepatol. 24 (4) (2009) 672–680.
[39] A.C. Ford, B.E. Lacy, L.A. Harris, et al., Effect of antidepressants and psychological therapies in irritable bowel syndrome: an updated systematic review and meta-analysis, Am. J. Gastroenterol. 114 (1) (2019) 21–39.
[40] B. Bonaz, R.D. Lane, M.L. Oshinsky, et al., Diseases, disorders, and comorbidities of interoception, Trends Neurosci. 44 (1) (2021) 39–51.
[41] M.R. Blake, J.M. Raker, K. Whelan, Validity and reliability of the Bristol Stool Form Scale in healthy adults and patients with diarrhoea-predominant irritable bowel syndrome, Aliment. Pharmacol. Ther. 44 (7) (2016) 693–703.
[42] M.H. Farzaei, R. Bahramsoltani, M. Abdollahi, et al., The role of visceral hypersensitivity in irritable bowel syndrome: pharmacological targets and novel treatments, J Neurogastroenterol Motil 22 (4) (2016) 558–574.
[43] R.C. Benvenutti, C.A. Dalla Vecchia, G. Locateli, et al., Gastroprotective activity of hydroalcoholic extract of the leaves of Urera baccifera in rodents, J. Ethnopharmacol. 250 (2020), 112473.
[44] X.Q. Sun, X.B. Fu, R. Zhang, et al., Relationship between plasma D(-)-lactate and intestinal damage after severe injuries in rats, World J. Gastroenterol. 7 (4) (2001 Aug) 555–558.
[45] B. Xia, W. Wu, W. Fang, et al., Heat stress-induced mucosal barrier dysfunction is potentially associated with gut microbiota dysbiosis in pigs, Anim Nutr 8 (1) (2022) 289–299.
[46] C. Pellegrini, L. Antonioli, G. Lopez-Castejon, et al., Canonical and non-canonical activation of NLRP3 inflammasome at the crossroad between immune tolerance and intestinal inflammation, Front. Immunol. 8 (2017) 36.
[47] Q.Y. Gu, J. Zhang, Y.C. Feng, Role of NLRP3 inflammasome in Bifidobacterium longum-regulated visceral hypersensitivity of postinfectious irritable bowel syndrome, Artif. Cell Nanomed. Biotechnol. 44 (8) (2016) 1933–1937.
[48] F. Awad, E. Assrawi, C. Louvrier, et al., Inflammasome biology, molecular pathology and therapeutic implications, Pharmacol. Ther. 187 (2018) 133–149.
[49] S. Vallabhapurapu, M. Karin, Regulation and function of NF-kappaB transcription factors in the immune system, Annu. Rev. Immunol. 27 (2009) 693–733.
[50] U. Heinemann, A. Schuetz, Structural features of tight-junction proteins, Int. J. Mol. Sci. 20 (23) (2019) 6020.
[51] C. Barmeyer, J.D. Schulzke, M. Fromm, Claudin-related intestinal diseases, Semin. Cell Dev. Biol. 42 (2015) 30–38.
[52] K. Sugita, K. Kabashima, Tight junctions in the development of asthma, chronic rhinosinusitis, atopic dermatitis, eosinophilic esophagitis, and inflammatory bowel diseases, J. Leukoc. Biol. 107 (5) (2020) 749–762.
[53] T. Suzuki, Regulation of intestinal epithelial permeability by tight junctions, Cell. Mol. Life Sci. 70 (4) (2013) 631–659.
[54] M. Rawat, M. Nighot, R. Al-Sadi, et al., IL1B increases intestinal tight junction permeability by up-regulation of MIR200C-3p, which degrades occludin mRNA, Gastroenterology 159 (4) (2020) 1375–1389.
[55] C. Martinez, B.K. Rodino-Janeiro, B. Lobo, et al., miR-16 and miR-125b are involved in barrier function dysregulation through the modulation of claudin-2 and cingulin expression in the jejunum in IBS with diarrhoea, Gut 66 (9) (2017) 1537–1538.